# Joint Channel Estimation and Impulsive Noise Mitigation in Underwater Acoustic OFDM Communication Systems

Peng Chen, Yue Rong, *Senior Member, IEEE*, Sven Nordholm, *Senior Member, IEEE*, Zhiqiang He, *Member, IEEE*, and Alexander J. Duncan, *Member, IEEE*

*Abstract*—Impulsive noise occurs frequently in underwater acoustic (UA) channels and can significantly degrade the performance of UA orthogonal frequency-division multiplexing (OFDM) systems. In this paper, we propose two novel compressed sensing based algorithms for joint channel estimation and impulsive noise mitigation in UA OFDM systems. The first algorithm jointly estimates the channel impulse response and the impulsive noise by utilizing pilot subcarriers. The estimated impulsive noise is then converted to the time domain and removed from the received signals. We show that this algorithm reduces the system bit-error-rate through improved channel estimation and impulsive noise mitigation. In the second proposed algorithm, a joint estimation of the channel impulse response and the impulsive noise is performed by exploiting the initially detected data. Then, the estimated impulsive noise is removed from the received signals. The proposed algorithms are evaluated and compared with existing methods through numerical simulations and on real data collected during a UA communication experiment conducted in the estuary of the Swan River, WA, Australia, during December 2015. The results show that the proposed approaches consistently improve the accuracy of channel estimation and the performance of impulsive noise mitigation in UA OFDM communication systems.

*Index Terms*—Underwater acoustic communication, OFDM, impulsive noise, compressed sensing.

## I. INTRODUCTION

THE underwater acoustic (UA) channel, especially the shallow water UA channel, is one of the most challenging channels for wireless communication, due to its extremely limited bandwidth, severe fading, strong multipath interference, and significant Doppler shifts [1]. The UA channel introduces dispersion to signals in both time and frequency domains. The time-domain dispersion due to large delay spread results in severe inter-symbol interference (ISI). The frequency-domain dispersion caused by the drift of the transmitter and receiver and the motion of the sea surface leads to a rapidly time-varying channel [1], [2]. In the past decades, significant advances have been made in high data rate UA communications [3]–[7]. Among them, UA orthogonal frequency-division multiplexing (OFDM) systems have attracted much research interest, due to their strong capability in mitigating ISI with a large delay spread [8]–[12].

In addition to the above challenges, UA communication is also impacted by impulsive noise introduced by natural sources and human activities [13]–[16]. Natural sources of impulsive noise include bio-acoustic sounds such as snapping shrimp and dolphins, water agitation (e.g. breaking waves and rainfall near the sea surface), and crustal movement such as earthquakes at the sea bed. Impulsive noise from human activities is usually generated by shipping, oil and gas exploration and production, and sonar related applications. Impulsive noise affects both the low (10 Hz to 500 Hz) and medium (500 Hz to 25 kHz) frequency bands used for UA communication. It is reported in [13] that impulsive noise can significantly degrade the performance of UA OFDM systems.

Impulsive noise mitigation for OFDM systems has been studied in power line communications [17]–[21]. Recently, this topic received increasing attention in UA communications [13], [22]–[24]. In general, there are two classes of impulsive noise suppression algorithms. Firstly, compared with the background noise, impulsive noise usually arrives randomly with a short duration and consists of very high power impulses. One can adopt nonlinear operations such as clipping and blanking [25], [26] to suppress the impulsive noise. In this class of approaches, the received signals are passed through a filter where the samples possibly contaminated by impulsive noise are first found via a thresholding test and then either deleted (blanking) or kept at a maximal amplitude level (clipping). In general, these algorithms can be used for both single-carrier and multicarrier systems. However, for OFDM systems, it is often difficult to choose a proper threshold of the nonlinear operation which sufficiently suppresses the impulsive noise without distorting the OFDM signal.

Another class of impulsive noise mitigation algorithms exploit the sparsity of impulsive noise [16], [27] and the structure of OFDM signals. These algorithms first estimate the impulsive noise from the null and/or pilot subcarriers, and then subtract the estimated impulsive noise from the received signals. These algorithms usually assume static or semi-static channel impulse responses which are known to the receiver [19] or only use null subcarriers to avoid the need for channel knowledge when estimating the impulsive noise [18], [22], [23]. However, the UA channel is rapidly time-varying and the limited bandwidth restricts the number of null subcarriers available.

Joint channel and impulsive noise estimation has been investigated in [28] by using the compressed sensing (CS) technique based on the following assumptions: (1) There are no impulsive noise samples within the maximum delay of the channel impulse response. (2) All symbols in the pilot sequence have identical phase. However, these two assumptions are hard to meet in practical UA communication systems. In [21], the generalized approximate message passing technique has been applied to jointly estimate the channel coefficients, impulsive noise, and the data symbols. However, the algorithm in [21] requires a priori information about the channel impulse response and the impulsive noise which depends heavily on the UA environment and is hard to obtain in advance.

In this paper, we propose two novel CS based algorithms for joint channel estimation and impulsive noise mitigation in UA OFDM systems by exploiting the sparsity of both the UA channel and the impulsive noise. It has been shown in [29] that many shallow water UA channels have a sparse structure, which means that although the UA channel impulse response generally has an extremely large delay spread, most of the channel energy is carried by only a few propagation paths. By exploiting the sparsity of the UA channel impulse response, channel estimators at the receiver can have a reduced number of taps, which reduces the noise involved in channel estimation. Consequently, the channel estimation can have an improved accuracy and reduced computational complexity [6], [30].

The first proposed algorithm utilizes the pilot subcarriers to jointly estimate the channel impulse response and the impulsive noise. We show that this algorithm successfully improves the accuracy of channel estimation, as the existence of impulsive noise is explicitly considered during channel estimation. Once the impulsive noise is estimated using the pilot subcarriers, it is transformed to the time domain and removed from the received signals before channel equalization. We propose two approaches, namely the least-squares (LS) based approach and the discrete Fourier transform (DFT) based method to perform such a transformation. Interestingly, we show that the LS based approach provides a better performance, while the DFT based method has a lower computational complexity.

In the second proposed algorithm, we use the data detected after the initial channel equalization to improve the estimation of the channel impulse response and impulsive noise. Then the estimated impulsive noise is removed from the received signals. Compared with the first algorithm, the advantage of
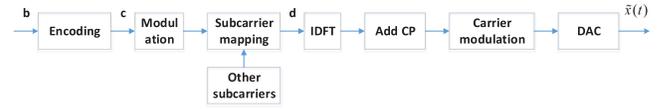


Fig. 1.    Block diagram of the transmitter in a UA OFDM communication system.

the second approach is that both the data and pilot subcarriers are utilized for channel estimation and impulsive noise mitigation. As many impulsive noise mitigation algorithms for wireless, underwater acoustic, and powerline OFDM systems use the null subcarriers [18], [22], [23], the algorithms proposed in this paper provide novel solutions for joint channel estimation and impulsive noise mitigation. Numerical simulations show that compared with existing methods, the proposed algorithms have a better mean-squared error (MSE) performance in channel estimation and yield a lower system bit-error-rate (BER). Both proposed algorithms are applied to process the data collected during the UA communication experiment conducted in December 2015 in the estuary of the Swan River, Western Australia. The results show that the proposed approaches are able to mitigate the impulsive noise in UA OFDM communication systems and improve the accuracy of channel estimation.

The rest of the paper is organized as follows. The system model is presented in Section II. In Section III, the proposed joint channel estimation and impulsive noise mitigation algorithms are presented. Numerical simulation and experimental results are shown in Section IV and Section V, respectively, to verify the performance of the proposed algorithms, and conclusions are drawn in Section VI.

## II. SYSTEM MODEL

In this paper, we consider a frame based coded UA OFDM communication system. As shown in Fig. 1, at the transmitter end, in each frame, a binary source data stream $\boldsymbol{b} = (b[1], \ldots, b[L_b])^T$ is encoded, interleaved, and punctured to form a coded sequence $\boldsymbol{c} = (c[1], \ldots, c[L_c])^T$ with length $L_c = R_m N_s N_b$, where $(\cdot)^T$ denotes the matrix (vector) transpose, $L_b$ is the number of information-carrying bits in each frame, $R_m$ denotes the modulation order, $N_s$ is the number of data subcarriers, and $N_b$ denotes the number of OFDM blocks in one frame. Note that as the algorithms to be presented are independent of the channel coding scheme, any codes (such as the turbo code and the convolutional code) can be used. The coded sequence $\boldsymbol{c}$ is mapped into $N_s N_b$ data symbols taken from the phase-shift keying (PSK) or quadrature amplitude modulation (QAM) constellations. Then every $N_s$ data symbols together with $N_p$ quadrature PSK (QPSK) modulated pilot symbols are mapped into one OFDM symbol vector $\boldsymbol{d} = (d[1], \ldots, d[N_c])^T$, where $N_p$ and $N_c \geq N_p + N_s$ are the number of pilot subcarriers and total subcarriers, respectively. We denote $\mathfrak{I}_d$ and $\mathfrak{I}_p$ as the indices of subcarriers with data symbols and pilot symbols, respectively. We assume that pilot subcarriers are uniformly spaced and denote $\boldsymbol{d}_p$ as the pilot sequence in one OFDM block.

Passband signals are directly generated for each OFDM block at the transmitter. Let $f_{sc}$ denote the subcarrier spacing. The bandwidth of the transmitted signal is $B = f_{sc}N_c$ and the duration of one OFDM symbol is $T = 1/f_{sc}$. The $N_c$ subcarriers are located at frequencies

$$f_k = f_c + kf_{sc}, \ k = -\frac{N_c}{2} + 1, \ldots, \frac{N_c}{2}$$

where $f_c$ is the center carrier frequency. To enable simple one-tap equalization and to avoid interference among OFDM blocks, a cyclic prefix (CP) of length $T_{cp}$ is prepended to the OFDM symbol, and the total length of one OFDM block is $T_{total} = T + T_{cp}$. The continuous time representation of an OFDM block can be expressed as

$$\tilde{x}(t) = 2\text{Re} \left\{ \left[ \frac{1}{\sqrt{N_c}} \sum_{k=-\frac{N_c}{2}+1}^{\frac{N_c}{2}} \check{d}[k]e^{j2\pi kf_{sc}t} \right] e^{j2\pi f_c t} \right\},$$
$$0 \le t \le T$$

$$\tilde{x}(t) = \tilde{x}(t + T), \quad -T_{cp} \le t < 0 \tag{1}$$

where $\text{Re}\{\cdot\}$ denotes the real part of a complex number and

$$\check{d}[k] = \begin{cases} d[k], & 1 \le k \le \frac{N_c}{2} \\ d[k + N_c], & -\frac{N_c}{2} + 1 \le k \le 0. \end{cases}$$

A general UA channel with $L_p$ paths can be represented as

$$h(t, \tau) = \sum_{l=1}^{L_p} A_l(t)\delta(t - \tau_l(t)) \tag{2}$$

where $A_l(t)$ and $\tau_l(t)$ are the amplitude and delay of the $l$th path, respectively, and we assume $T_{cp} > \tau_{L_p}(t)$. In general, UA communication suffers from time-varying frequency offset caused by the variation of $\tau_l(t)$ within one OFDM block. Similar to [23], we assume that $A_l(t)$ is constant and all paths have the same Doppler scaling factor $a$ during one OFDM block.[1] Thus

$$\tau_l(t) \approx \tau_l - at, \quad l = 1, \ldots, L_p.$$

Then the received passband signal of one OFDM block is given by

$$\tilde{r}(t) = \sum_{l=1}^{L_p} A_l \tilde{x}(t - \tau_l + at) + \tilde{v}(t) + \tilde{w}(t) \tag{3}$$

where $\tilde{v}(t)$ is the passband impulsive noise and $\tilde{w}(t)$ represents other non-impulsive background noise. A resampling factor $\hat{a}$ is estimated and used to resample the received signal. After removing the CP, downshifting, and low-pass filtering, the baseband received signal can be obtained

from (1) and (3) as

$$r(t) \approx e^{j2\pi\check{a}t} \sum_{l=1}^{L_p} \frac{A_l e^{-j2\pi f_c \tau_l}}{\sqrt{N_c}} \sum_{k=-\frac{N_c}{2}+1}^{\frac{N_c}{2}} \check{d}[k]e^{j2\pi kf_{sc}(t-\tau_l)}$$
$$+ v(t) + w(t)$$
$$= e^{j2\pi\check{a}t} \frac{1}{\sqrt{N_c}} \sum_{k=-\frac{N_c}{2}+1}^{\frac{N_c}{2}} \check{d}[k]e^{j2\pi kf_{sc}t} \sum_{l=1}^{L_p} A_l e^{-j2\pi f_k \tau_l}$$
$$+ v(t) + w(t), \ 0 \le t \le T \tag{4}$$

where $\check{a} = f_c(a - \hat{a})/(1 + \hat{a})$ represents the frequency offset introduced by the Doppler shift, $v(t)$ and $w(t)$ are the baseband impulsive noise and other noise, respectively. From (4), the channel frequency response at the $k$th subcarrier is given by

$$H[k] = \sum_{l=1}^{L_p} A_l e^{-j2\pi f_k \tau_l}, \quad k = -\frac{N_c}{2} + 1, \ldots, \frac{N_c}{2}.$$

By sampling $r(t)$ at the rate of $1/B$, we obtain discrete time samples of one OFDM symbol from (4) as

$$r[i] = \frac{e^{j2\pi i\check{a}/B}}{\sqrt{N_c}} \sum_{k=-\frac{N_c}{2}+1}^{\frac{N_c}{2}} \check{d}[k]e^{j2\pi ikf_{sc}/B} H[k] + v[i] + w[i]$$
$$= \frac{e^{j2\pi i\check{a}/B}}{\sqrt{N_c}} \sum_{k=-\frac{N_c}{2}+1}^{\frac{N_c}{2}} \check{d}[k]e^{j2\pi ik/N_c} H[k] + v[i] + w[i],$$
$$i = 1, \ldots, N_c \tag{5}$$

where $v[i]$ and $w[i]$ are the impulsive noise and other noise samples, respectively. The matrix-vector form of (5) is given by

$$\boldsymbol{r} = \boldsymbol{\Phi F^H D h}_f + \boldsymbol{v} + \boldsymbol{w}$$
$$= \boldsymbol{\Phi F^H D F h}_t + \boldsymbol{v} + \boldsymbol{w} \tag{6}$$

where $(\cdot)^H$ denotes the conjugate transpose, $\boldsymbol{D} = \text{diag}(\boldsymbol{d})$ is a diagonal matrix taking $\boldsymbol{d}$ as the main diagonal elements, $\boldsymbol{\Phi} = \text{diag}(e^{j2\pi\check{a}/B}, \cdots, e^{j2\pi N_c\check{a}/B})$, $\boldsymbol{r} = (r[1], \ldots, r[N_c])^T$, $\boldsymbol{v} = (v[1], \ldots, v[N_c])^T$, $\boldsymbol{w} = (w[1], \ldots, w[N_c])^T$, $\boldsymbol{F}$ is an $N_c \times N_c$ discrete Fourier transform (DFT) matrix with the $(i, k)$-th entry of $1/\sqrt{N_c}e^{-j2\pi (i-1)(k-1)/N_c}$, $i, k = 1, \ldots, N_c$. In (6), $\boldsymbol{h}_f = (h_f[1], \ldots, h_f[N_c])^T$ is a vector containing the channel frequency response at all $N_c$ subcarriers with

$$h_f[k] = \begin{cases} H[k], & 1 \le k \le \frac{N_c}{2} \\ H[k - N_c], & \frac{N_c}{2} + 1 \le k \le N_c \end{cases}$$

and $\boldsymbol{h}_t = \boldsymbol{F^H h}_f$ is the discrete time domain representation of the channel impulse response with a maximum delay of $L_m = \lceil B\tau_{L_p} \rceil$.

We adopt the "clipping-blanking and Doppler" algorithm in [23] to estimate and compensate the frequency offset $\check{a}$, which essentially performs the Doppler shift estimation using the method in [31, Sec. 3.1] on the blanked version of $\boldsymbol{r}$. Note that after this frequency offset compensation, there may

exist a small value of residual frequency offset, due to the mismatch between the true frequency offset and its estimated value. The effect of such residual frequency offset will be discussed in Section IV-C, where we show that the impact of residual frequency offset on the system BER performance is negligible. After removing the frequency offset from (6), the frequency domain representation of the received signal can be written as

$$r_f = FF^H Dh_f + Fv + Fw$$
$$= Dh_f + v_f + w_f \tag{7}$$

where $v_f = Fv$ and $w_f = Fw$ are the impulsive noise and other noise in the frequency domain, respectively.

## III. PROPOSED APPROACHES

In this section, we propose two CS based algorithms for joint channel estimation and impulsive noise mitigation in UA OFDM communication systems. We first give a brief introduction of the CS technique, which will be used in the proposed algorithms.

### A. Compressed Sensing Technique

CS is a technique that can recover signal accurately from its measurements provided that the signal is sparse [32]. Let us consider the measurement model of

$$y = Ax + n$$

where the dimensions of $y$ and $x$ are $M \times 1$ and $L \times 1$, respectively.

When $M < L$, it is hard to apply conventional estimation methods such as the LS and the minimum mean-squared error (MMSE) estimators to recover $x$ from $y$. However, if $x$ is $S$-sparse, which means that $x$ has only $S < L$ non-zero entries, and $A$ is designed to capture the dominant information of $x$ into $y$, then $x$ can be recovered by the CS technique. To ensure $y$ contains the main information of $x$ and the recovery procedure works properly, the measurement matrix $A$ should satisfy some properties such as the restricted isometric property [33] or the coherence property [34].

Many algorithms such as orthogonal matching pursuit (OMP), basis pursuit (BP), and compressed sampling matching pursuit (CoSaMP) have been developed for sparse signal recovery. In this paper, the OMP algorithm [36] is adopted. The procedure of the OMP algorithm is shown in Table I, where $(\cdot)^{-1}$ stands for the matrix inversion, the superscript $(s)$ denotes the variables at the $s$th iteration, and $A[:, p]$ denotes the $p$th column of $A$.

### B. Pilot Subcarriers Based Impulsive Noise Cancelation

The block diagram of various receivers is shown in Fig. 2, where CE denotes channel estimation and JCINE stands for the proposed joint channel and impulsive noise estimation algorithm. The proposed receivers correspond to branches labeled with (c), (d), and (e) in Fig. 2.

### TABLE I
### PROCEDURE OF THE OMP ALGORITHM

Initialization
$\hat{x} = 0, z^{(0)} = y, u^{(0)} = \varnothing, \bar{A}^{(0)} = \varnothing$

For $s = 1, \cdots, S$
  Calculate the correlation vector $b^{(s)} = A^H z^{(s-1)}$
  Find the index $q = \arg\max_{j=1,\ldots,L, j \notin u^{(s-1)}} b^{(s)}[j]$
  Update the index set $u^{(s)} = u^{(s-1)} \cup q$
  Update $\bar{A}^{(s)} = \bar{A}^{(s-1)} \cup A[:, q]$
  Update $\bar{x} = ((\bar{A}^{(s)})^H \bar{A}^{(s)})^{-1} (\bar{A}^{(s)})^H y$
  Update the residual measurement
  $z^{(s)} = y - \bar{A}^{(s)} \bar{x}$
end for
$\hat{x}[u^{(S)}[i]] = \bar{x}[i], i = 1, \ldots, S.$
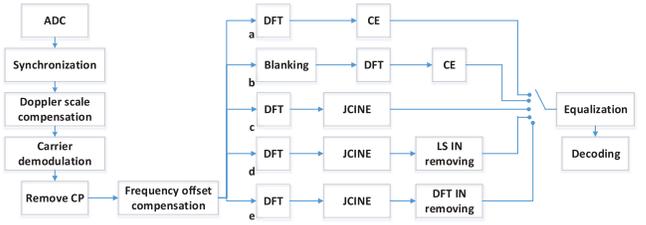


Fig. 2. Block diagram of various receivers.

*1) Compressive Sensing Based Joint Channel and Impulsive Noise Estimation:* Let us introduce an $N_p \times N_c$ matrix $P$ which selects $N_p$ pilot subcarriers out of total $N_c$ subcarriers. Thus, $P$ has unit entry at the $(i, \mathfrak{I}_p[i])$-th position, $i = 1, \cdots, N_p$, and zero elsewhere. From (7), the received signals in the pilot subcarriers can be written as

$$r_p = PDh_f + Pv_f + Pw_f$$
$$= D_p h_p + v_p + w_p$$
$$= D_p F_p h_{p,t} + F_p v_{p,t} + w_p$$
$$= M_p \alpha_p + w_p \tag{8}$$

where $D_p = \text{diag}(d_p)$, $h_p$ contains the channel frequency responses at $N_p$ pilot subcarriers, $F_p$ is an $N_p \times N_p$ DFT matrix with the $(i, k)$-th entry of $1/\sqrt{N_p} e^{-j2\pi (i-1)(k-1)/N_p}$, $i, k = 1, \ldots, N_p$, and

$$v_p = Pv_f, \quad w_p = Pw_f, \quad h_{p,t} = F_p^H h_p, \quad v_{p,t} = F_p^H v_p$$
$$\alpha_p = (h_{p,t}^T, v_{p,t}^T)^T, \quad M_p = (D_p F_p, F_p). \tag{9}$$

We select $N_p \geq L_m$, which means that all the non-zero entries of $h_t$ are within its first $N_p$ entries. In this case, $h_t$ can be easily recovered from $h_{p,t}$. Interestingly, for the special case of $N_c = K N_p$ and $\mathfrak{I}_p[i] = (i-1)K + 1, i = 1, \ldots, N_p$, where $K$ is an integer, there is $h_t = [\sqrt{K} h_{p,t}^T, 0_{1 \times (N_c - N_p)}]^T$. Since the UA channel is sparse, only a few entries of $h_{p,t}$ are non-zero. Moreover, $v_{p,t}$ can be viewed as a 'fold-and-add' version of $v$ which is considered to be sparse as well. Therefore, it is reasonable to assume that $\alpha_p$ is sparse.

As the dimension of $M_p$ is $N_p \times 2N_p$, it is hard to recover $\alpha_p$ from $r_p$ using conventional LS and MMSE estimators. However, by exploiting the sparsity of $\alpha_p$, we can apply compressed sensing techniques to obtain an accurate estimation of $\alpha_p$. In Appendix A, we show that the coherence

between columns of $M_p$ is very small. Thus, the OMP method [36] can be adopted here to estimate $\alpha_p$ [30].

We would like to mention that as the existence of impulsive noise is explicitly considered by (8) during channel estimation, the proposed joint channel and impulsive noise estimation algorithm improves the accuracy of channel estimation. Let $\hat{\alpha}_p = (\hat{h}_{p,t}^T, \ \hat{v}_{p,t}^T)^T$ denote the estimated $\alpha_p$. From (8), the estimated channel frequency response in the pilot subcarriers can be obtained by

$$\hat{h}_p = F_p \hat{h}_{p,t}. \tag{10}$$

One can use the improved channel estimation result in (10) to perform channel equalization as indicated by the branch marked with (c) in Fig. 2. The performance of this approach will be studied in Sections IV and V.

The non-zero entries of $h_t$ are all located within its first $N_p$ entries, whereas the non-zero entries of the impulsive noise $v$ can appear at any of the $N_c$ entries. Since $v_{p,t}$ is a 'fold-and-add' version of $v$, to obtain an estimation of $v$ from $v_{p,t}$, the positions of the impulsive noise need to be known in general. This can be done by a thresholding test, where the receiver firstly calculates the average power $G$ of the current OFDM block and then collects the positions of possible impulsive noise into a vector $\mathcal{I}_I$ which satisfies

$$|r[\mathcal{I}_I[i]]|^2 > G\beta, \quad i = 1, \ldots, N_I. \tag{11}$$

Here $\beta$ is a threshold parameter [35] and $N_I$ is the number of possible positions of impulsive noise. Then two approaches can be used to estimate $v$ based on $\hat{v}_{p,t}$ as discussed below.

Note that the original OMP algorithm in Table I does not take into account the detected impulsive noise positions. To exploit these positions, we develop an enhanced joint channel and impulsive noise estimation algorithm (EJCINE) algorithm. In this algorithm, the receiver maps the positions in $\mathcal{I}_I$ to their corresponding positions in $v_{p,t}$ similar to the approach in Appendix B. Let us denote the mapping results as $\mathcal{I}_s$. When using the OMP algorithm to jointly estimate the channel and impulsive noise in Table I, we set $u^{(0)} = \mathcal{I}_s$ and choose $\bar{A}^{(0)}$ to be the corresponding columns of $A$ indicated by $\mathcal{I}_s$.

*2) Least-Squares Based Impulsive Noise Cancelation:* Let us introduce $v_I$ as a vector which contains all the $N_I$ samples of impulsive noise in one OFDM block. Then the impact of $v_I$ on the $N_p$ pilot subcarriers can be written as

$$v_p = PFP_I v_I \tag{12}$$

where $P_I$ is an $N_c \times N_I$ matrix indicating the position of the impulsive noise given by

$$P_I[i,k] = \begin{cases} 1, & i = \mathcal{I}_I[k], \ k = 1, \ldots, N_I \\ 0, & \text{otherwise.} \end{cases}$$

Note that an estimation of $v_p$ can be obtained from (8) as

$$\hat{v}_p = F_p \hat{v}_{p,t}. \tag{13}$$

Thus, using (12) and (13), $v_I$ can be estimated as

$$\begin{aligned} \hat{v}_I &= (F_I^H F_I)^{-1} F_I^H \hat{v}_p \\ &= (F_I^H F_I)^{-1} F_I^H F_p \hat{v}_{p,t} \end{aligned} \tag{14}$$

where $F_I = PFP_I$. Then $v$ is estimated by $\hat{v} = P_I \hat{v}_I$. Finally, $\hat{v}$ is subtracted from the received signal $r$ as in branch (d) in Fig. 2 and the resulting signals are passed to channel equalization and decoding operations.

*3) DFT Based Impulsive Noise Cancelation:* When $N_c = KN_p$, in addition to the LS based method presented above, a DFT based approach can also be applied for impulsive noise cancelation, which has a lower computational complexity than the LS based method. Let us denote $m_p$ ($1 \le m_p \le K$) as the index of the first pilot subcarrier. The pilot subcarriers selection matrix $P$ is given by

$$P[i,k] = \begin{cases} 1, & k = (i-1)K + m_p, \ i = 1, \ldots, N_p \\ 0, & \text{otherwise.} \end{cases}$$

By transforming $v_p$ into the time domain, we have

$$\begin{aligned} n &= KF^H P^T v_p \\ &= KF^H P^T PFv \\ &= KF^H \bar{P}Fv \end{aligned} \tag{15}$$

where $\bar{P} = P^T P$ is an $N_c \times N_c$ matrix with unit entry at $\bar{P}[i,i]$, $i = mK + m_p, m = 0, \ldots, N_p - 1$. We show in Appendix B that the $(MN_p + Q)$-th entry of $n$, $M = 0, \ldots, K-1$, $Q = 1, \ldots, N_p$, is given by

$$n[MN_p + Q] = \sum_{h=0}^{K-1} e^{\frac{j2\pi(M-h)(m_p-1)}{K}} v[hN_p + Q]. \tag{16}$$

It can be seen from (16) that each entry of $n$ is the sum of $K$ phase-shifted entries of $v$. However, because of the sparsity of $v$, it is with high possibility that, at most, only one of these $K$ entries is non-zero when $K$ is small (Typically, $K = 4$ or $6$ in UA OFDM systems).[2] Based on the above assumption and the fact that $v[i] \ne 0$ for $i \in \mathcal{I}_I$, an estimation of $v$ can be obtained by

$$\hat{v}[i] = \begin{cases} \hat{n}[i], & i \in \mathcal{I}_I \\ 0, & \text{otherwise} \end{cases}$$

where $\hat{n}$ is the estimated $n$ as shown below.

From (13) and (15), we have

$$\begin{aligned} \hat{n} &= KF^H P^T \hat{v}_p \\ &= KF^H P^T F_p \hat{v}_{p,t}. \end{aligned}$$

Then the $(i = MN_p + Q)$-th entry of $\hat{n}$ can be expressed as

$$\begin{aligned} \hat{n}[i] &= KF^H[i,:]P^T F_p \hat{v}_{p,t} \\ &= \frac{\sqrt{K}}{N_p} \sum_{m=1}^{N_p} \sum_{l=1}^{N_p} \sum_{k=1}^{N_c} e^{\frac{j2\pi(i-1)(k-1)}{N_c}} P[l,k] e^{\frac{-j2\pi(l-1)(m-1)}{N_p}} \hat{v}_{p,t}[m] \\ &= \frac{\sqrt{K}}{N_p} \sum_{m=1}^{N_p} \sum_{l=1}^{N_p} e^{\frac{j2\pi(i-1)((l-1)K+m_p-1)}{N_c}} e^{\frac{-j2\pi(l-1)(m-1)}{N_p}} \hat{v}_{p,t}[m] \\ &= \frac{\sqrt{K}}{N_p} \sum_{m=1}^{N_p} e^{\frac{j2\pi(i-1)(m_p-1)}{N_c}} \hat{v}_{p,t}[m] \sum_{l=1}^{N_p} e^{\frac{j2\pi(l-1)(i-m)}{N_p}} \\ &= \frac{\sqrt{K}}{N_p} \sum_{m=1}^{N_p} e^{\frac{j2\pi(i-1)(m_p-1)}{N_c}} \hat{v}_{p,t}[m] \sum_{l=1}^{N_p} e^{\frac{j2\pi(l-1)(MN_p+Q-m)}{N_p}} \\ &= \sqrt{K} e^{\frac{j2\pi(i-1)(m_p-1)}{N_c}} \hat{v}_{p,t}[Q] \end{aligned} \tag{17}$$

---

[2]The impact of the low probability case when more than one of these $K$ entries are non-zero on the system performance is small, as shown in Section V-C.
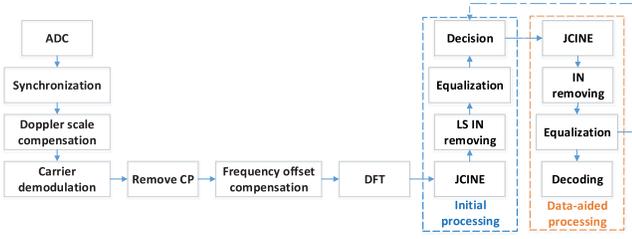
Fig. 3.    Block diagram of the data-aided joint channel estimation and impulsive noise cancelation algorithm.

where to obtain the last equation, we used the fact that

$$\sum_{l=1}^{N_p} e^{\frac{j2\pi \ (l-1)(MN_p+Q-m)}{N_p}} = \begin{cases} N_p, & m = Q \\ 0, & m \neq Q. \end{cases}$$

Based on (16) and (17), we have

$$\hat{v}[i] = \begin{cases} \sqrt{K} e^{\frac{j2\pi \ (i-1)(m_p-1)}{N_c}} \hat{v}_{p,t}[i|N_p], & i \in \mathcal{I}_I \\ 0, & \text{otherwise} \end{cases} \quad (18)$$

where $(\cdot|\cdot)$ is the modulo operator. Finally, $\hat{v}$ is subtracted from the received signal $r$ as in branch (e) in Fig. 2 and the resulting signals are passed to channel equalization and decoding operations.

It can be seen from (18) that an estimation of $v$ can be obtained from $\hat{v}_{p,t}$ after simple scaling and phase rotation, whereas matrix inversion (14) is required in the LS-based approach to estimate $v$ from $\hat{v}_{p,t}$. Thus, the DFT-based impulsive noise cancelation method has a lower complexity than the LS-based one.

### C. Data-Aided Joint Channel Estimation and Impulsive Noise Cancelation

A data-aided processing as shown in Fig. 3 can further improve the system performance after the JCINE and the impulsive noise removal operations in Section III-B. For the simplicity of presentation, the LS based approach in Section III-B2 is used for impulsive noise cancelation in the initial processing. By using (10) and the interpolation operation, an estimation of $h_f$ can be obtained and used to equalize the received signals $r_f$ (7) in the initial processing. Then hard decision can be applied to the equalizer output to obtain the estimated data symbols, and together with $d_p$, an estimation of $d$ can be obtained. Similar to (8), we obtain from (7) that

$$\begin{aligned} r_f &= \hat{D} F h_t + F v + \bar{w}_f \\ &= M \alpha + \bar{w}_f \end{aligned} \quad (19)$$

where $\hat{D} = \text{diag}(\hat{d})$, $\hat{d}$ is an estimation of $d$ from the initial processing, $\alpha = (h_t^T, \ v^T)^T$, $M = (\hat{D}F, \ F)$, and $\bar{w}_f = w_f + (D - \hat{D}) F h_t$. Similar to Section III-B, we show in Appendix C that the coherence between columns of $M$ is very small. Thus, we can adopt a compressed sensing method, for example the OMP method [36], to estimate the sparse vector $\alpha$. Note that as both the data and pilot subcarriers are utilized in (19), the estimation of $h_t$ and $v$ is more accurate than that

in Section III-B, provided that the mismatch between $d$ and $\hat{d}$ is small.

Let us introduce $\hat{\alpha} = (\hat{h}_t^T, \ \hat{v}^T)^T$ as the estimated $\alpha$. The estimated impulsive noise can be removed from the received signals as $\bar{r}_f = r_f - F\hat{v}$, and the channel estimation result can be updated by $\hat{h}_f = F\hat{h}_t$. Then $\bar{r}_f$ and $\hat{h}_f$ are used to perform channel equalization and decoding. It will be seen in Sections IV and V-C that the data-aided receiver has a significantly improved performance compared with the initial processing, at the price of a higher computational complexity. We would like to note that the data-aided joint channel estimation and impulsive noise cancelation process can be carried out iteratively, as indicated by the dashed arrow in Fig. 3, to improve the receiver decoding performance. Interestingly, we show through numerical simulations in Section IV-E that the gain of the second iteration over the first iteration is marginal.

## IV. SIMULATION RESULTS

### A. Simulation Setup

In this section, we study the performance of the proposed algorithms through numerical simulations. We simulate a UA OFDM system with 512 subcarriers including 325 data subcarriers, 128 uniformly spaced pilot subcarriers for channel estimation, and 59 null subcarriers. Each OFDM block contains a 100-sample long CP. Five OFDM blocks are transmitted in each channel realization and the simulation results are averaged through $10^4$ channel realizations. The pilot symbols are modulated by QPSK constellations, and the data symbols are modulated by 1/2 rate turbo encoded QPSK constellations. Considering the code puncturing, the number of information-carrying bits in each channel realization is $L_b = 1632$.

The system bandwidth is 4 kHz. Thus, the bandwidth of each subcarrier is 7.8 Hz. Unless explicitly mentioned, the frequency offset is randomly generated between $-5$ Hz and 5 Hz, which is typical in UA communication systems. We simulate a UA channel with 15 paths. The arrival times of all paths follow a Poisson distribution with an average delay of 1 ms between two adjacent paths. The amplitudes of the paths are Rayleigh distributed with variances following an exponentially decreasing profile. The ratio of the channel variances between the start and the end of the CP is 20 dB.

Let $v = v + w$ represent the total additive noise in (6). A two-component Gaussian mixture (GM) model [23] is used to generate $v$ with a probability density function of

$$f(v[i]) = (1-q)\mathcal{N}(0, \sigma^2) + q\mathcal{N}(0, \sigma_I^2), \ i = 1, \ldots, N_c \quad (20)$$

where $\mathcal{N}(0, \cdot)$ denotes a zero-mean complex Gaussian distribution function, $\sigma^2$ is the variance of the background (non-impulsive) noise, $\sigma_I^2$ is the variance of the impulsive noise, and $q$ is the probability of occurrence of the impulsive noise. We define the signal-to-non-impulsive noise ratio (SNR) as $\text{SNR} = P_s/\sigma^2$ and the signal-to-impulsive noise ratio (SIR) as $\text{SIR} = P_s/\sigma_I^2$, where $P_s$ is the power of the transmitted signal. In the simulations, similar to [23], we choose $q = 0.02$. We vary the SNR and SIR to investigate the performance of the proposed algorithms.
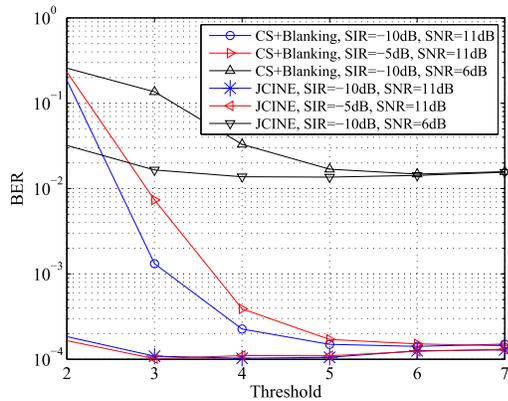
Fig. 4.   BER versus threshold.



Fig. 5.   Impact of frequency offset estimation on the system BER performance.

## B. Threshold Selection

We first study the impact of $\beta$ (11) on the system performance. Fig. 4 shows the system coded BER versus $\beta$ at three SNR and SIR combinations: SNR = 11dB with SIR = −10dB, SNR = 11dB with SIR = −5dB, and SNR = 6dB with SIR = −10dB, yielded by the proposed JCINE algorithm with the LS-based impulsive noise cancelation (INC) and the "CS+blanking" approach. In the latter approach, the blanking method is used to remove the samples $r[i]$ at positions determined by $\mathcal{I}_I$ in (11), and the OMP algorithm is used for channel estimation.

It can be seen from Fig. 4 that the proposed JCINE algorithm is more robust than the CS+blanking approach in choosing $\beta$. This is due to the fact that the proposed algorithm estimates and removes the impulsive noise instead of erasing both the impulsive noise and the useful signal on the selected samples. Thus, with a lower threshold $\beta$, the blanking algorithm is more likely to delete samples with large amplitude which are in fact not affected by impulsive noise, while the proposed JCINE algorithm only selects those samples but never deletes them. We can also observe from Fig. 4 that the best choice of $\beta$ for the JCINE algorithm is around 4. While for the CS+blanking algorithm, a good $\beta$ can be selected between 4 and 7, with the best choice between 5 and 6. In the following, we choose $\beta = 5$ for the simulations and experiments, which in fact tests the performance of the proposed algorithm in a harsher way than the blanking approach.

## C. Frequency Offset Mitigation

We investigate the effect of residual frequency offset (after the frequency offset compensation described in Section II) by checking the system coded BER performance. The CS+blanking algorithm is adopted here to detect the received signals. We compare the system BER performance under the following three scenarios.

- Non-frequency offset (FO): The received signals are affected by impulsive noise, but the frequency offset is set to zero. This serves as a benchmark for the system BER performance without any frequency offset.
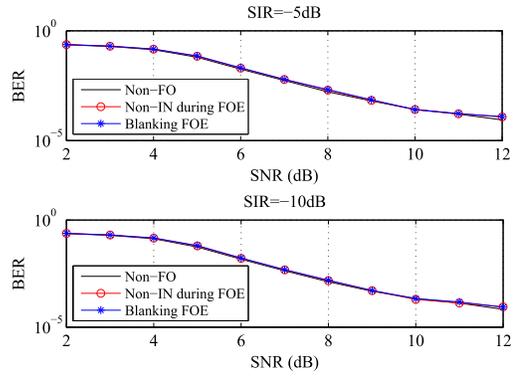
- Non-impulsive noise (IN) during the frequency offset estimation (FOE): The received signals are not contaminated by impulsive noise during the frequency offset estimation and compensation process.
- Blanking FOE: The received signals suffer from both the impulsive noise and frequency offset. The frequency offset estimation is performed after the blanking operation with a step size of 0.2 Hz [23].

Fig. 5 shows the system coded BER versus SNR for the three scenarios above at SIR= −5 dB and SIR= −10 dB. Interestingly, it can be seen from Fig. 5 that the system BERs in the three scenarios are almost identical. This indicates that: (1) The frequency offset estimation is reliable after the blanking operation, as the frequency offset estimation with and without impulsive noise yields similar BER; (2) The residual frequency offset is not the main factor that limits the system performance [37], because after frequency offset estimation and compensation, the system has a similar BER to that of the system without any frequency offset.

## D. Channel Estimation Results

In this subsection, we study the channel estimation performance of the proposed algorithms. As we focus on the channel estimation results, the frequency offset is set to zero in this simulation. The MSE of channel estimation is defined as

$$\text{MSE} = \text{E} \left\{ \frac{(\hat{\boldsymbol{h}}_f - \boldsymbol{h}_f)^H (\hat{\boldsymbol{h}}_f - \boldsymbol{h}_f)}{\boldsymbol{h}_f^H \boldsymbol{h}_f} \right\} \quad (21)$$

where $\text{E}\{\cdot\}$ denotes the statistical expectation and $\hat{\boldsymbol{h}}_f$ is the estimation of the true channel $\boldsymbol{h}_f$.

Fig. 6 shows the MSE of four algorithms versus SNR at SIR= −10 dB, where "LS+blanking" refers to the approach that the blanking method is used to remove the samples $r[i]$ at positions determined by $\mathcal{I}_I$ in (11), followed by the OMP algorithm for channel estimation. "DA JCINE" refers to the data-aided (DA) JCINE algorithm developed in Section III-C. It can be seen from Fig. 6 that the CS-based channel estimation algorithms significantly outperform the LS-based channel estimation. The proposed JCINE algorithms have a better channel estimation performance than the blanking-based approaches, as the blanking operation introduces noise when
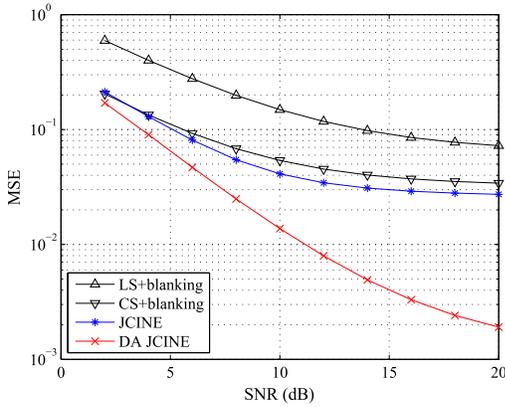
Fig. 6.   MSE of channel estimation versus SNR.



Fig. 7.   BER versus SNR at SIR $= -5$ dB.

deleting the selected samples. Moreover, the proposed data-aided JCINE algorithm significantly improves the precision of channel estimation, because this algorithm further suppresses the impulsive noise and at the same time explores the data subcarriers for channel estimation.

It can also be observed from Fig. 6 that the MSEs of channel estimation decrease slower at high SNRs. This can be explained by the fact that as SNR increases, the power of the non-impulsive noise decreases, making the impulsive noise a more significant factor limiting the channel estimation performance.

### E. BER Performance Results

We compare the system BER performance for the following algorithms.

- Ideal case: The frequency offset is set to zero and there is no impulsive noise in the simulation. Moreover, the receiver has perfect channel knowledge. Obviously, this provides a lower bound of BER for practical receiver algorithms.
- Non-FO non-IN CS: The frequency offset is set to zero and no impulsive noise exists in the simulation. Moreover, the OMP algorithm is used for channel estimation.
- LS+blanking: Explained in Section IV-D.
- CS+blanking: Explained in Section IV-B.
- JCINE+LS INC: Explained in Section IV-B.
- JCINE+DFT INC: The proposed JCINE algorithm with DFT-based impulsive noise cancelation.
- EJCINE+LS INC: The EJCINE algorithm proposed in Section III-B with LS-based impulsive noise cancelation.
- EJCINE P + LS INC: The EJCINE algorithm assuming known impulsive noise positions with LS-based impulsive noise cancelation.
- DA JCINE: Explained in Section IV-D.
- CS+CS: CS-based channel estimation and impulsive noise mitigation using the pilot and null subcarriers, respectively.

Figs. 7 and 8 demonstrate the BERs of the above algorithms versus SNR at SIR$= -5$ dB and SIR$= -10$ dB, respectively. It can be seen that the CS-based channel estimation algorithms outperform the LS-based approach. The
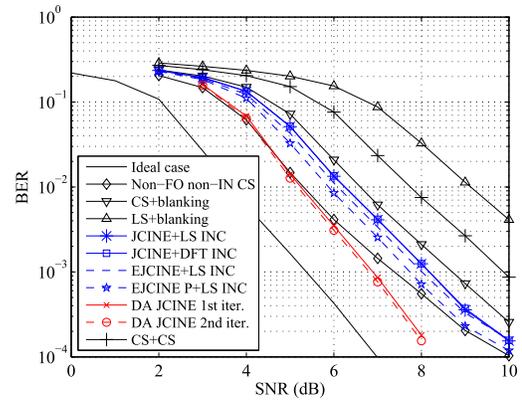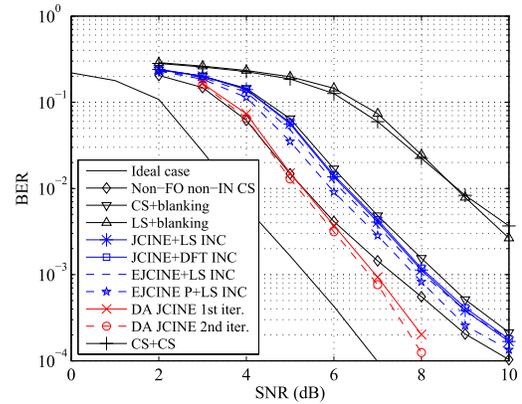


Fig. 8.   BER versus SNR at SIR $= -10$ dB.

proposed algorithms have smaller BERs than the CS+blanking and CS+CS approaches. Moreover, the SNR gain of the JCINE algorithm over the CS+blanking approach is larger at higher SIR.

We can also observe from Figs. 7 and 8 that by exploiting the detected impulsive noise positions when carrying out the OMP algorithm, the EJCINE algorithm can slightly improve the system BER performance. It is worth noting that the data-aided JCINE algorithm greatly reduces the system BER, particularly at high SNRs, where it yields a smaller BER than the non-FO non-IN CS scenario. This is due to the fact that this algorithm further suppresses the impulsive noise and explores the data subcarriers for channel estimation. Interestingly, for the data-aided JCINE algorithm, the gain of the second iteration over the first iteration is small. Considering that the second iteration greatly increases the computational complexity, one iteration would be sufficient in practical UA communication systems.

Fig. 9 shows the BERs of five algorithms versus SIR at SNR=7 dB. It can be seen that the proposed algorithms have constant BER performance for a wide range of SIR, which demonstrates the strong capability of the proposed algorithms in mitigating different levels of impulsive noise. We can also observe from Fig. 9 that the gap between the first and second iterations of the DA JCINE algorithm remains unchanged over the SIRs tested.
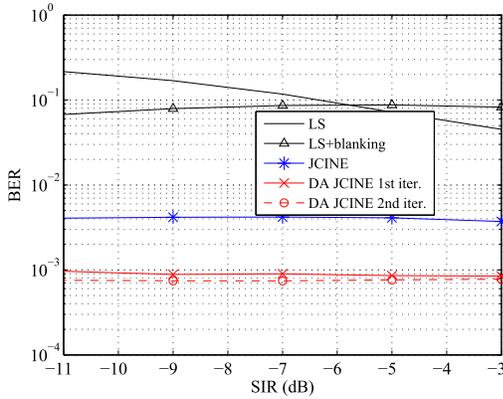
Fig. 9.  BER versus SIR at SNR = 7 dB.



Fig. 10.  Transmitter and receiver locations during the experiment.

## V. EXPERIMENT RESULTS AND DISCUSSIONS

In this section, we apply the proposed algorithms to process the data recorded during a UA communication experiment conducted in December 2015 in the estuary of the Swan River, Western Australia.

### A. Experiment Arrangement

The locations of the transmitter and receiver are shown in Fig. 10, where the distance between the transmitter and receiver was 936 meters. The water depth along the direct path varied between 2.5 and 6 meters, which was very shallow. Both the transmitter transducer and the receiver hydrophone were mounted 0.5 meter above the river bed on steel frames and were cabled to shore. The water depths at the transmitter and the receiver were 5 meters and 2.5 meters, respectively. The movement of the hydrophone and the transducer was small as they were attached to steel frames. As the hydrophone was located in warm shallow water close to a jetty, there was a significant amount of highly impulsive snapping shrimp noise. Another source of impulsive noise during the experiment was from waves breaking at the jetty piers, the intensity of which increases with the wind speed. To investigate the impact of wind on the breaking wave noise, the same data file was transmitted three times during the day at different wind conditions.

Key parameters of the experimental system are summarized in Table II. Fig. 11 illustrates the frame structure of the

TABLE II
EXPERIMENTAL SYSTEM PARAMETERS

| Number of OFDM blocks | $N_b$ | 5 |
|---|---|---|
| Bandwidth | $B$ | 4 kHz |
| Carrier frequency | $f_c$ | 12 kHz |
| Sampling rate | $f_s$ | 96 kHz |
| Number of subcarriers | $N_c$ | 512 |
| Subcarrier spacing | $f_{sc}$ | 7.8 Hz |
| Length of OFDM symbol | $T$ | 128 ms |
| Length of CP | $T_{cp}$ | 25 ms |
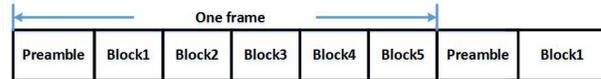


Fig. 11.  Frame structure of the transmitted signals.
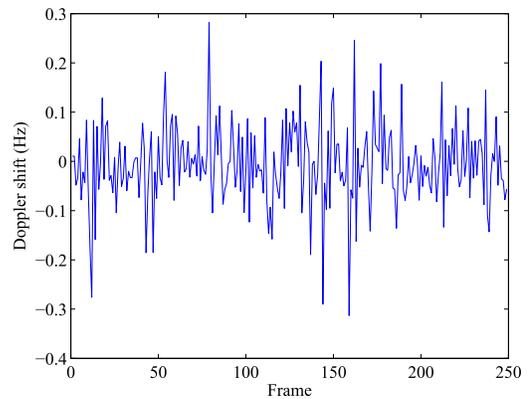


Fig. 12.  Doppler shift estimated by the preamble blocks in the T83 file.

transmitted signals. It can be seen that each frame contains $N_b = 5$ OFDM data blocks and one preamble block. The preamble block has $N_c$ subcarriers, half of which are null subcarriers and the other half are pilot subcarriers. For data blocks, among the total 512 subcarriers, there are 325 data subcarriers, 128 uniformly spaced pilot subcarriers for channel estimation, 18 null subcarriers at each edge of the passband, and 23 subcarriers for frequency offset estimation. The pilot symbols are modulated by QPSK constellations. The data symbols are modulated by either QPSK constellations encoded by 1/2 or 1/3 rate turbo codes or 16-QAM constellations with a 1/3 rate turbo code. Considering the code puncturing, the number of information-carrying bits in each frame is $L_b = 1632$ (QPSK, 1/2 rate), $L_b = 1088$ (QPSK, 1/3 rate), or $L_b = 2167$ (16-QAM). Thus, the system source data rate is

$$R_b = \frac{L_b}{(T+T_{cp})(N_b+1)} = \begin{cases} 1.19 \text{ kb/s} & \text{QPSK, 1/3 rate} \\ 1.78 \text{ kb/s} & \text{QPSK, 1/2 rate} \\ 2.36 \text{ kb/s} & \text{16-QAM, 1/3 rate.} \end{cases}$$

Each transmission contains 750 frames with 250 frames for every modulation type. The data files recorded at the receiver during three transmissions were named T83, T84, and T85, respectively.
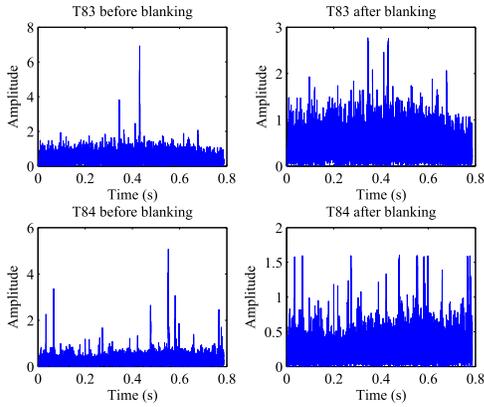
Fig. 13. Amplitude of the received signals in a typical frame of the T83 and the T84 files.



Fig. 14. Amplitude of channel impulse response estimated by the preamble blocks in the T83 file.

TABLE III
ESTIMATED SIR AND SNR

| File | MCC | SIR (dB) | SNR (dB) | $q$ |
|------|-----|----------|----------|-----|
| T83 | QPSK 1/3 rate | -8.0 | 10.2 | 2.1% |
| | QPSK 1/2 rate | -6.8 | 10.8 | 2.1% |
| | 16-QAM 1/3 rate | -5.7 | 12.0 | 1.8% |
| T84 | QPSK 1/3 rate | -13.1 | 5.4 | 2.4% |
| | QPSK 1/2 rate | -12.5 | 5.3 | 2.5% |
| | 16-QAM 1/3 rate | -14.6 | 4.0 | 2.4% |
| T85 | QPSK 1/3 rate | -13.3 | 8.3 | 1.8% |
| | QPSK 1/2 rate | -13.2 | 7.6 | 2.1% |
| | 16-QAM 1/3 rate | -11.7 | 7.8 | 2.4% |

## B. Channel Conditions

As the transmitter and receiver were attached to fixed steel frames, the channel Doppler shift was small during the experiment. Fig. 12 shows the Doppler shift estimated by the preamble block in each frame of the T83 file. It can be seen that as the Doppler shift of most of the frames is smaller than 0.2 Hz, the step of Doppler shift compensation can be skipped when processing the received data. This has been justified in Section IV-C and Fig. 5, as the residual frequency offset is not the main factor that limits the system performance.

Among the three recorded data files, the T84 file contains signals most heavily affected by the impulsive noise, while signals in the T83 file are least impacted by the impulsive noise. The amplitude of the received signals in a typical data frame taken from the T83 and the T84 files is shown in Fig. 13. It can be seen that even after the blanking operation, there is still significant amount of impulsive noise in the T84 file. In fact, due to the dense impulsive noise, the synchronization algorithm failed to find the head of 9 data frames (4, 2, and 3 frames in the 1/3 rate QPSK, 1/2 rate QPSK, and 16-QAM modulated signals, respectively) in the T84 file. The estimated SIR, SNR, and the impulsive noise occurrence probability $q$ of the data in three files are shown in Table III for various modulation type and coding rate combinations (MCC).

To study the channel conditions, we perform channel estimation using the preamble blocks based on the LS estimator. Fig. 14 illustrates the amplitude of the estimated channel impulse responses of several data frames in the T83 file where the preamble blocks have only slight interference from the
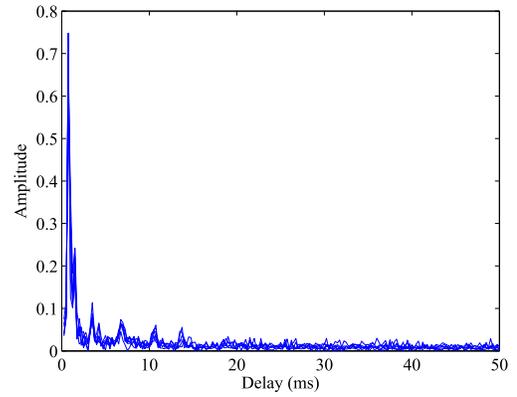
impulsive noise. It can be seen that in this case, the channel estimation result is reasonable. In particular, we can observe from Fig. 14 that the maximal channel delay spread in the experiment is about 15 ms which is shorter than the length of the CP. Moreover, it can be seen that there are seven notable paths between the transmitter and the receiver.

## C. Receiver Performance for QPSK Modulated Signals

The BER (both raw and coded) and the frame-error-rate (FER) performances of various algorithms with QPSK modulated signals are shown in Tables IV–VI for three recorded files. To calculate the FER, one frame is considered erroneous if one or more of the $L_b$ information-carrying bits in this frame is incorrectly decoded. The BER and FER performances of the following channel estimation and interference mitigation algorithms are compared.

- LS channel estimator without the blanking operation (branch (a) in Fig. 2).
- LS channel estimator after blanking of the impulsive samples detected at the positions of $\mathfrak{I}_I$ (11) (branch (b) in Fig. 2).
- CS channel estimator after blanking of the impulsive samples detected at the positions of $\mathfrak{I}_I$ (11) (branch (b) in Fig. 2).
- Proposed JCINE algorithm without INC (branch (c) in Fig. 2).
- Proposed JCINE algorithm with the DFT based INC (branch (e) in Fig. 2).
- Proposed JCINE algorithm with the LS based INC (branch (d) in Fig. 2).
- Proposed data-aided INC (Section III-C).

It can be seen from Tables IV–VI that compared with the LS estimator without the blanking operation, the proposed JCINE algorithm without impulsive noise cancelation can reduce the raw (uncoded) BER by around 1% for the T83 file and 2% for the T84 and T85 files, and the coded BER by 3-4% for the T84 file and 6% for the T85 file with 1/2 coding rate. Such performance gain is mainly contributed by an improved channel estimation using the JCINE algorithm, where the existence of impulsive noise is explicitly considered during channel estimation (8). Interestingly, it can be seen from

TABLE IV
PERFORMANCE COMPARISON OF VARIOUS ALGORITHMS
FOR THE T83 FILE (QPSK MODULATION)

| Coding rate | Method | Raw BER | Coded BER | FER |
|---|---|---|---|---|
| 1/3 | LS w/o blanking | 6.2% | 0.2% | 0.4% |
| | LS + blanking | 5.2% | 0 | 0 |
| | JCINE w/o INC | 5.0% | 0 | 0 |
| | JCINE + DFT INC | 3.5% | 0 | 0 |
| | JCINE + LS INC | 3.5% | 0 | 0 |
| | Data-aided INC | 2.1% | 0 | 0 |
| 1/2 | LS w/o blanking | 5.6% | 0.3% | 1.6% |
| | LS + blanking | 4.7% | 0 | 0 |
| | JCINE w/o INC | 4.6% | 0 | 0 |
| | JCINE + DFT INC | 3.3% | 0 | 0 |
| | JCINE + LS INC | 3.3% | 0 | 0 |
| | Data-aided INC | 2.1% | 0 | 0 |

TABLE V
PERFORMANCE COMPARISON OF VARIOUS ALGORITHMS
FOR THE T84 FILE (QPSK MODULATION)

| Coding rate | Method | Raw BER | Coded BER | FER |
|---|---|---|---|---|
| 1/3 | LS w/o blanking | 18.7% | 10.9% | 50.4% |
| | LS + blanking | 15.5% | 1.3% | 7.3% |
| | JCINE w/o INC | 16.7% | 6.5% | 30.5% |
| | JCINE + DFT INC | 14.8% | 0.6% | 4.1% |
| | JCINE + LS INC | 14.7% | 0.5% | 4.1% |
| | Data-aided INC | 11.6% | 0.02% | 0.4% |
| 1/2 | LS w/o blanking | 18.1% | 22.5% | 93.6% |
| | LS + blanking | 14.6% | 15.9% | 84.7% |
| | JCINE w/o INC | 16.0% | 19.3% | 87.9% |
| | JCINE + DFT INC | 13.5% | 11.1% | 62.9% |
| | JCINE + LS INC | 13.5% | 10.9% | 61.7% |
| | Data-aided INC | 11.1% | 3.0% | 21.0% |

TABLE VI
PERFORMANCE COMPARISON OF VARIOUS ALGORITHMS
FOR THE T85 FILE (QPSK MODULATION)

| Coding rate | Method | Raw BER | Coded BER | FER |
|---|---|---|---|---|
| 1/3 | LS w/o blanking | 13.5% | 1.6% | 6.4% |
| | LS + blanking | 11.2% | 0 | 0 |
| | JCINE w/o INC | 11.6% | 0.7% | 2.4% |
| | JCINE + DFT INC | 9.1% | 0 | 0 |
| | JCINE + LS INC | 9.1% | 0 | 0 |
| | Data-aided INC | 6.8% | 0 | 0 |
| 1/2 | LS w/o blanking | 15.0% | 15.3% | 71.6% |
| | LS + blanking | 11.7% | 3.9% | 24.8% |
| | JCINE w/o INC | 12.8% | 9.5% | 50.8% |
| | JCINE + DFT INC | 9.9% | 0.7% | 5.6% |
| | JCINE + LS INC | 9.8% | 0.5% | 5.2% |
| | Data-aided INC | 7.4% | 0 | 0 |

Table IV that as the T83 file is only slightly affected by impulsive noise, an improved channel estimation together with channel coding are sufficient to obtain zero coded BER and FER over the investigated data.

The impulsive noise cancelation step after the JCINE algorithm can further improve the system performance. It can be seen from Tables V and VI that compared with the JCINE algorithm without impulsive noise cancelation, around 2-3% reduction in the raw BER has been achieved for both the T84 and T85 files. Moreover, 6% reduction (T84 file, 1/3 rate) and 9% reduction (T84 and T85 files, 1/2 rate) in the coded BER have been achieved with the impulsive noise cancelation step. We observe that both the LS based impulsive noise cancelation approach in Section III-B2 and the

TABLE VII
PERFORMANCE COMPARISON OF VARIOUS ALGORITHMS
FOR 16-QAM MODULATED SIGNALS

| File | Method | Raw BER | Coded BER | FER |
|---|---|---|---|---|
| T83 | LS w/o blanking | 10.0% | 0.01% | 0.4% |
| | LS + blanking | 10.0% | 0 | 0 |
| | JCINE w/o INC | 9.7% | 0 | 0 |
| | JCINE + LS INC | 8.2% | 0 | 0 |
| | Data-aided INC | 6.7% | 0 | 0 |
| T84 | LS w/o blanking | 31.2% | 35.5% | 100% |
| | LS + blanking | 27.9% | 32.0% | 100% |
| | JCINE w/o INC | 30.1% | 34.2% | 100% |
| | JCINE + LS INC | 27.6% | 30.6% | 100% |
| | Data-aided INC | 26.3% | 27.1% | 97.6% |
| T85 | LS w/o blanking | 25.9% | 25.5% | 90.0% |
| | LS + blanking | 23.6% | 19.0% | 76.4% |
| | CS + blanking | 22.5% | 7.2% | 41.2% |
| | JCINE w/o INC | 24.4% | 20.5% | 75.6% |
| | JCINE + LS INC | 21.4% | 4.3% | 22.8% |
| | Data-aided INC (1 It.) | 20.2% | 1.8% | 11.2% |
| | Data-aided INC (2 It.) | 20.0% | 1.7% | 10.8% |

DFT based one in Section III-B3 outperform the LS blanking based impulsive noise cancelation method, indicating that the lower BER and FER of the proposed JCINE+INC algorithm compared with the LS+blanking method is a result of both a more accurate channel estimation and a better impulsive noise cancelation. It can also been seen from Tables V and VI that the JCINE algorithm with impulsive noise cancelation significantly reduces the system FER.

Interestingly, we can see from Tables IV–VI that the DFT based impulsive noise cancelation approach has only slightly worse BER and FER performances than the LS based one. This is caused by the low probability case that more than one of the $K$ entries of $v[hN_p + P]$, $h = 0, \cdots, K-1$, in (16) are non-zero. However, the DFT based impulsive noise cancelation approach has a much lower computational complexity as the receiver can reconstruct the impulsive noise directly from the estimation of $v_{p,t}$ as in (18), while matrix inversion (14) needs to be performed in the LS based approach. Such performance-complexity tradeoff is very useful for practical UA OFDM systems.

From Tables IV–VI we can see that the data-aided impulsive noise cancelation approach significantly improves the system BER and FER performances in all three files. Compared with the blanking method, a further improvement of 3-4% in the raw BER and more than 10% reduction in the coded BER (1/2 rate) have been achieved in the T84 file. For the T85 file, a reducing of 4% in the coded BER is observed with 1/2 rate. Such performance improvement is mainly achieved through improved channel and impulsive noise estimation obtained by using both the data and pilot subcarriers.

### D. Receiver Performance for 16-QAM Modulated Signals

The BER and FER performances of various algorithms with 16-QAM modulated signals are shown in Table VII. Similar to the case of QPSK modulated signals, it can be seen from Table VII that the proposed JCINE algorithm without impulsive noise cancelation has a better performance than the LS method without blanking. As expected, for the blanking

method, CS-based channel estimation has a better performance than the LS-base method. The impulsive noise cancelation step after the JCINE algorithm outperforms both the LS and CS methods with blanking.

We also observe from Table VII that the data-aided impulsive noise cancelation approach further improves the system BER and FER performances, particulary for the T85 file. Compared with the LS method with blanking, the proposed data-aided algorithm reduces the raw BER by around 3% and the coded BER by 13% for the T85 file. The above benefits indicate that the data-aided algorithm is able to mitigate the impact of impulsive noise in UA OFDM systems with non-constant amplitude source signals (such as QAM-modulated signals). It can be seen that compared with the first iteration, only a marginal BER and FER reduction is achieved after the second iteration of the data-aided algorithm.

As the T84 file is severely contaminated by impulsive noise, it can be seen from Table VII that although the proposed algorithms successfully reduce the raw and coded BER, the system FER remains high, indicating that the channel condition of T84 is very challenging for 16-QAM modulated signals.

## VI. Conclusions

We have proposed two novel joint channel estimation and impulsive noise mitigation algorithms for UA OFDM systems. By utilizing only the pilot subcarriers, the first algorithm successfully improves the accuracy of channel estimation and the performance of impulsive noise mitigation. Based on the data detected from the first algorithm, the second algorithm applies the data-aided processing to further improve the performance of channel estimation and impulsive noise cancelation by exploiting both the data and pilot subcarriers. We have shown that the measurement matrices in both algorithms have small coherence between columns, so that the compressed sensing technique can be applied in both proposed algorithms. The proposed algorithms are applied to process the data collected during a recent UA communication experiment. The results show that when the received signals are only slightly influenced by impulsive noise, the first algorithm without impulsive noise canceling is sufficient to achieve a low system BER. When the received signals are severely impacted by impulsive noise, the impulsive noise cancelation step of the first algorithm and the second method can be adopted to significantly improve the system BER performance.

## APPENDIX A
### COHERENCE PROPERTY OF $M_p$

It follows from (9) that as the pilot symbols are QPSK modulated, there is

$$
\begin{aligned}
C_p &= M_p^H M_p \\
&= (D_p F_p \quad F_p)^H (D_p F_p \quad F_p) \\
&= \begin{bmatrix} F_p^H D_p^H D_p F_p & F_p^H D_p^H F_p \\ F_p^H D_p F_p & F_p^H F_p \end{bmatrix} \\
&= \begin{bmatrix} I_{N_p} & F_p^H D_p^H F_p \\ F_p^H D_p F_p & I_{N_p} \end{bmatrix}
\end{aligned}
\tag{22}
$$

where $I_n$ stands for an $n \times n$ identity matrix. From (22) we find that any column of $M_p$ satisfies $\|M_p[:, i]\| = 1$, where $\| \cdot \|$ stands for the vector Euclidean norm.

Since $D_p$ is a diagonal matrix, the $(l, m)$-th entry of $C_f = F_p^H D_p F_p$ is given by

$$
\begin{aligned}
C_f[l, m] &= \sum_{i=1}^{N_p} F_p^H[l, i] d_p[i] F_p[i, m] \\
&= \frac{1}{N_p} \sum_{i=1}^{N_p} e^{j2\pi li/N_p} d_p[i] e^{-j2\pi mi/N_p} \\
&= \frac{1}{N_p} \sum_{i=1}^{N_p} e^{j2\pi(l-m)i/N_p} d_p[i].
\end{aligned}
\tag{23}
$$

We can design $d_p$ such that $|C_f[l, m]| \ll 1, l, m = 1, \cdots, N_p$ when $N_p$ is sufficiently large. Thus any two columns $M_p[:, l]$ and $M_p[:, m]$ satisfy

$$
\frac{|M_p^H[:, l] M_p[:, m]|}{\|M_p[:, l]\| \, \|M_p[:, m]\|} \ll 1
$$

which indicates that the coherence between columns of $M_p$ is very small.

## APPENDIX B
### PROOF OF (16)

Let us introduce $i = M N_p + Q$. From (15), we have

$$
\begin{aligned}
n[i] &= K F^H[i, :] \bar{P} F v \\
&= \frac{K}{N_c} \sum_{l=1}^{N_c} \sum_{k=1}^{N_c} e^{j2\pi \frac{(i-1)(k-1)}{N_c}} \bar{P}[k, k] e^{-j2\pi \frac{(k-1)(l-1)}{N_c}} v[l] \\
&= \frac{K}{N_c} \sum_{l=1}^{N_c} \sum_{k=1}^{N_c} e^{j2\pi \frac{(i-l)(k-1)}{N_c}} \bar{P}[k, k] v[l] \\
&= \frac{K}{N_c} \sum_{l=1}^{N_c} \sum_{m=0}^{N_p-1} e^{j2\pi \frac{(i-l)(mK+m_p-1)}{N_c}} v[l] \\
&= \frac{1}{N_p} \sum_{l=1}^{N_c} e^{j2\pi \frac{(i-l)(m_p-1)}{N_c}} v[l] \sum_{m=0}^{N_p-1} e^{j2\pi \frac{(i-l)mK}{KN_p}} \\
&= \frac{1}{N_p} \sum_{h=0}^{K-1} \sum_{p=1}^{N_p} e^{j2\pi \frac{(MN_p+Q-(hN_p+p))(m_p-1)}{KN_p}} \\
&\quad \times v[hN_p + p] \sum_{m=0}^{N_p-1} e^{j2\pi \frac{(MN_p+Q-(hN_p+p))m}{N_p}} \\
&= \sum_{h=0}^{K-1} e^{j2\pi \frac{(M-h)(m_p-1)}{K}} v[hN_p + Q]
\end{aligned}
$$

where we applied the fact that

$$
\sum_{m=0}^{N_p-1} e^{j2\pi \frac{(MN_p+Q-(hN_p+p))m}{N_p}} = \begin{cases} N_p, & p = Q \\ 0, & p \neq Q \end{cases}
$$

to obtain the last equation.

## Appendix C
### Coherence Property of $M$

From (19) we have

$$C_M = M^H M \tag{24}$$

$$= (\hat{D}F, \quad F)^H (\hat{D}F, \quad F)$$

$$= \begin{bmatrix} F^H \hat{D}^H \hat{D} F & F^H \hat{D}^H F \\ F^H \hat{D} F & F^H F \end{bmatrix}$$

$$= \begin{bmatrix} F^H \hat{D}^H \hat{D} F & F^H \hat{D}^H F \\ F^H \hat{D} F & I_{N_c} \end{bmatrix}. \tag{25}$$

The main difference between (22) and (25) is that the entries of $\hat{D}$ are not limited to QPSK constellations. They may, for example, be taken from QAM constellations. Similar to (23), for $C_d = F^H \hat{D} F$, we have

$$C_d[l, m] = \frac{1}{N_c} \sum_{i=1}^{N_c} e^{j2\pi(l-m)i/N_c} \hat{d}[i]. \tag{26}$$

Because the elements of $\hat{d}$ are either well designed (pilot subcarriers) or independently generated symbols (data subcarriers), it is reasonable to assume that $C_d[l, m] \ll 1$, $l, m = 1, \ldots, N_c$.

For $C_g = F^H \hat{D}^H \hat{D} F$, we have

$$C_g[l, m] = \sum_{i=1}^{N_c} F^H[l, i] |\hat{d}[i]|^2 F[i, m]$$

$$= \frac{1}{N_c} \sum_{i=1}^{N_c} e^{\frac{j2\pi(l-1)(i-1)}{N_c}} |\hat{d}[i]|^2 e^{\frac{-j2\pi(i-1)(m-1)}{N_c}}$$

$$= \frac{1}{N_c} \sum_{i=1}^{N_c} e^{\frac{j2\pi(l-m)(i-1)}{N_c}} |\hat{d}[i]|^2. \tag{27}$$

Thus, $C_g[l, l] = \frac{1}{N_c} \sum_{i=1}^{N_c} |\hat{d}[i]|^2 \approx 1$ for $l = 1, \cdots, N_c$. Let us classify elements in $\hat{d}$ into a finite set $\mathcal{A}$ with a cardinality of $N_a$ according to their amplitude. For any $l \neq m$ we have from (27) that

$$C_g[l, m] = \frac{1}{N_c} \sum_{k=1}^{N_a} \sum_{|\hat{d}[i]|=\mathcal{A}[k]} e^{\frac{j2\pi(l-m)(i-1)}{N_c}} |\hat{d}[i]|^2$$

$$= \sum_{k=1}^{N_a} \frac{(\mathcal{A}[k])^2}{N_c} \sum_{|\hat{d}[i]|=\mathcal{A}[k]} e^{\frac{j2\pi(l-m)(i-1)}{N_c}}.$$

When $N_c \gg N_a$ we have $\frac{1}{N_c} \sum_{|\hat{d}[i]|=\mathcal{A}[k]} e^{\frac{j2\pi(l-m)(i-1)}{N_c}} \ll 1$ and hence $C_g[l, m] \ll 1$.

### Acknowledgement

### References

[1] D. B. Kilfoyle and A. B. Baggeroer, "The state of the art in underwater acoustic telemetry," *IEEE J. Ocean. Eng.*, vol. 25, no. 1, pp. 4–27, Jan. 2000.

[2] T. H. Eggen, A. B. Baggeroer, and J. C. Preisig, "Communication over Doppler spread channels—Part I: Channel and receiver presentation," *IEEE J. Ocean. Eng.*, vol. 25, no. 1, pp. 62–71, Jan. 2000.

[3] C. Bjerrum-Niese and R. Lutzen, "Stochastic simulation of acoustic communication in turbulent shallow water," *IEEE J. Ocean. Eng.*, vol. 25, no. 4, pp. 523–532, Oct. 2000.

[4] M. Stojanovic, J. Catipovic, and J. G. Proakis, "Adaptive multichannel combining and equalization for underwater acoustic communications," *J. Acoust. Soc. Amer.*, vol. 94, no. 3, pp. 1621–1631, Sep. 1993.

[5] M. Stojanovic and L. Freitag, "Multichannel detection for wideband underwater acoustic CDMA communications," *IEEE J. Ocean. Eng.*, vol. 31, no. 3, pp. 685–695, Jul. 2006.

[6] M. Stojanovic, L. Freitag, and M. Johnson, "Channel-estimation-based adaptive equalization of underwater acoustic signals," in *Proc. MTS/IEEE OCEANS*, vol. 2. Seattle, WA, USA, Sep. 1999, pp. 590–595.

[7] T. Öberg, B. Nilsson, N. Olofsson, M. L. Nordenvaad, and E. Sangfelt, "Underwater communication link with iterative equalization," in *Proc. MTS/IEEE OCEANS*, Boston, MA, USA, Sep. 2006, pp. 1–6.

[8] B. Li, S. Zhou, M. Stojanovic, and L. Freitag, "Pilot-tone based ZP-OFDM demodulation for an underwater acoustic channel," in *Proc. MTS/IEEE OCEANS*, Boston, MA, USA, Sep. 2006, pp. 1–5.

[9] M. Stojanovic, "Low complexity OFDM detector for underwater acoustic channels," in *Proc. MTS/IEEE OCEANS*, Boston, MA, USA, Sep. 2006, pp. 1–6.

[10] Z. Wang, S. Zhou, J. Catipovic, and P. Willett, "Asynchronous multiuser reception for OFDM in underwater acoustic communications," *IEEE Trans. Wireless Commun.*, vol. 12, no. 3, pp. 1050–1061, Mar. 2013.

[11] B. Li, S. Zhou, M. Stojanovic, L. Freitag, and P. Willett, "Multicarrier communication over underwater acoustic channels with nonuniform Doppler shifts," *IEEE J. Ocean. Eng.*, vol. 33, no. 2, pp. 198–209, Apr. 2008.

[12] H. Yan *et al.*, "DSP based receiver implementation for OFDM acoustic modems," *J. Phys. Commun.*, vol. 5, no. 1, pp. 22–32, Mar. 2012.

[13] M. Chitre, S. H. Ong, and J. Potter, "Performance of coded OFDM in very shallow water channels and snapping shrimp noise," in *Proc. MTS/IEEE OCEANS*, Washington, DC, USA, Sep. 2005, pp. 996–1001.

[14] M. Chitre, "A high-frequency warm shallow water acoustic communications channel model and measurements," *J. Acoust. Soc. Amer.*, vol. 122, no. 5, pp. 2580–2586, 2007.

[15] J. A. Hildebrand, "Anthropogenic and natural sources of ambient noise in the ocean," *Marine Ecol. Prog. Ser.*, vol. 395, pp. 5–20, Dec. 2009.

[16] M. Chitre, S. Kuselan, and V. Pallayil, "Ambient noise imaging in warm shallow waters; robust statistical algorithms and range estimation," *J. Acoust. Soc. Amer.*, vol. 132, no. 2, pp. 838–847, Aug. 2012.

[17] S. V. Zhidkov, "Analysis and comparison of several simple impulsive noise mitigation schemes for OFDM receivers," *IEEE Trans. Commun.*, vol. 56, no. 1, pp. 5–9, Jan. 2008.

[18] G. Caire, T. Y. Al-Naffouri, and A. K. Narayanan, "Impulse noise cancellation in OFDM: An application of compressed sensing," in *Proc. IEEE Int. Symp. Inf. Theory*, Toronto, ON, Canada, Jul. 2008, pp. 1293–1297.

[19] J. Lin, M. Nassar, and B. L. Evans, "Impulsive noise mitigation in powerline communications using sparse Bayesian learning," *IEEE J. Sel. Areas Commun.*, vol. 31, no. 7, pp. 1172–1183, Jul. 2013.

[20] A. Mengi and A. J. H. Vinck, "Successive impulsive noise suppression in OFDM," in *Proc. IEEE Int. Symp. Power Line Commun. Appl.*, Rio de Janeiro, Brazil, Mar. 2010, pp. 33–37.

[21] M. Nassar, P. Schniter, and B. L. Evans, "A factor graph approach to joint OFDM channel estimation and decoding in impulsive noise environments," *IEEE Trans. Signal Process.*, vol. 62, no. 6, pp. 1576–1589, Mar. 2014.

[22] H. Sun, W. Shen, Z. Wang, S. Zhou, X. Xu, and Y. Chen, "Joint carrier frequency offset and impulse noise estimation for underwater acoustic OFDM with null subcarriers," in *Proc. MTS/IEEE OCEANS*, Hampton Roads, VA, USA, Oct. 2012, pp. 1–4.

[23] X. Kuai, H. Sun, S. Zhou, and E. Cheng, "Impulsive noise mitigation in underwater acoustic OFDM systems," *IEEE Trans. Veh. Technol.*, vol. 65, no. 10, pp. 8190–8202, Oct. 2016.

[24] T. Suzuki, H. M. Tran, and T. Wada, "An underwater acoustic OFDM communication system with shrimp (impulsive) noise cancelling," in *Proc. Int. Conf. Comput., Manage., Telecommun.*, Da Nang, Vietnam, Apr. 2014, pp. 152–156.

[25] Y. H. Ma, P. L. So, and E. Gunawan, "Performance analysis of OFDM systems for broadband power line communications under impulsive noise and multipath effects," *IEEE Trans. Power Del.*, vol. 20, no. 2, pp. 674–681, Apr. 2005.

[26] S. Dimitrov, S. Sinanovic, and H. Haas, "Clipping noise in OFDM-based optical wireless communication systems," *IEEE Trans. Commun.*, vol. 60, no. 4, pp. 1072–1081, Apr. 2012.

[27] M. A. Chitre, J. R. Potter, and S. H. Ong, "Optimal and near-optimal signal detection in snapping shrimp dominated ambient noise," *IEEE J. Ocean. Eng.*, vol. 31, no. 2, pp. 497–503, Apr. 2006.

[28] A. Mehboob, L. Zhang, J. Khangosstar, and K. Suwunnapuk, "Joint channel and impulsive noise estimation for OFDM based power line communication systems using compressed sensing," in *Proc. IEEE Int. Symp. Power Line Commun. Appl.*, Johannesburg, South Africa, Mar. 2013, pp. 203–208.

[29] M. Stojanovic and J. Preisig, "Underwater acoustic communication channels: Propagation models and statistical characterization," *IEEE Commun. Mag.*, vol. 47, no. 1, pp. 84–89, Jan. 2009.

[30] W. Li and J. C. Preisig, "Estimation of rapidly time-varying sparse channels," *IEEE J. Ocean. Eng.*, vol. 32, no. 4, pp. 927–939, Oct. 2007.

[31] L. Wan, Z. Wang, S. Zhou, T. C. Yang, and Z. Shi, "Performance comparison of Doppler scale estimation methods for underwater acoustic OFDM," *J. Elect. Comput. Eng.*, vol. 2012, 2012, Art. no. 703243.

[32] E. J. Candès and M. B. Wakin, "An introduction to compressive sampling," *IEEE Signal Process. Mag.*, vol. 25, no. 2, pp. 21–30, Mar. 2008.

[33] E. J. Candès and Y. Plan, "A probabilistic and RIPless theory of compressed sensing," *IEEE Trans. Inf. Theory*, vol. 57, no. 11, pp. 7235–7254, Nov. 2011.

[34] M. F. Duarte and Y. C. Eldar, "Structured compressed sensing: From theory to applications," *IEEE Trans. Signal Process.*, vol. 59, no. 9, pp. 4053–4085, Sep. 2011.

[35] S. V. Zhidkov, "Performance analysis and optimization of OFDM receiver with blanking nonlinearity in impulsive noise environment," *IEEE Trans. Veh. Technol.*, vol. 55, no. 1, pp. 234–242, Jan. 2006.

[36] J. A. Tropp and A. C. Gilbert, "Signal recovery from random measurements via orthogonal matching pursuit," *IEEE Trans. Inf. Theory*, vol. 53, no. 12, pp. 4655–4666, Dec. 2007.

[37] S. F. Mason, C. R. Berger, S. Zhou, and P. Willett, "Detection, synchronization, and Doppler scale estimation with multicarrier waveforms in underwater acoustic communication," *IEEE J. Sel. Areas Commun.*, vol. 26, no. 9, pp. 1638–1649, Dec. 2008.

**Peng Chen** received the B.E. degree in information engineering and the Ph.D. degree in signal and information processing from the Beijing University of Posts and Telecommunications, China, in 2007 and 2013, respectively. He was a System Engineer with the Mobile Communication Division, Datang Mobile Communications Equipment Co. Ltd., Beijing, China, from 2013 to 2014. Since 2014, he has been with the Department of Electrical and Computer Engineering, Curtin University, Bentley, Australia, where he is currently a Research Associate. His research interests include signal processing, wireless communication systems, and channel estimation.
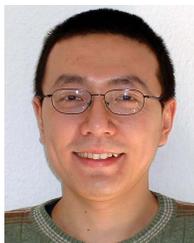


**Yue Rong** (S'03–M'06–SM'11) received the Ph.D. (*summa cum laude*) degree in electrical engineering from the Darmstadt University of Technology, Darmstadt, Germany, in 2005.

He was a Post-Doctoral Researcher with the Department of Electrical Engineering, University of California at Riverside, Riverside, CA, USA, from 2006 to 2007. Since 2007, he has been with the Department of Electrical and Computer Engineering, Curtin University, Bentley, Australia, where he is currently a Full Professor. His research interests include signal processing for communications, wireless communications, underwater acoustic communications, applications of linear algebra and optimization methods, and statistical and array signal processing. He has published over 140 journal and conference papers in these areas.

Dr. Rong was a TPC Member of the IEEE ICC, WCSP, IWCMC, EUSIPCO, and ChinaCom. He was a recipient of the Best Paper Award at the 2011 International Conference on Wireless Communications and Signal Processing, the Best Paper Award at the 2010 Asia-Pacific Conference on Communications, and the Young Researcher of the Year Award of the Faculty of Science and Engineering at Curtin University in 2010. He was an Editor of the IEEE WIRELESS COMMUNICATIONS LETTERS from 2012 to 2014, and a Guest Editor of the IEEE JOURNAL ON SELECTED AREAS IN COMMUNICATIONS Special Issue on Theories and Methods for Advanced Wireless Relays. He is an Associate Editor of the IEEE TRANSACTIONS ON SIGNAL PROCESSING.



**Sven Nordholm** (M'90–SM'05) received the M.Sc.E.E. (Civilingenjör) degree, the Licentiate of Engineering degree, and the Ph.D. degree in signal processing from Lund University, Sweden, in 1983, 1989, and 1992, respectively. Since 1999, he has been a Professor of signal processing with the Department of Electrical and Computer Engineering, Curtin University. From 1999 to 2002, he was the Director of ATRI. From 2002 to 2009, he was the Director of the Signal Processing Laboratory, WATRI, Western Australian Telecommunication Research Institute, a joint institute between The University of Western Australia and Curtin University. He is a Co-Founder of the start-up companies Sensear, providing voice communication in extreme noise conditions and Nuheara, a hearables company. He is a member of the IEEE TC AASP and an Associate Editor of the IEEE/ACM TASPL.

He has written over 200 papers in refereed journals and conference proceedings. He contributes frequently in book chapters and encyclopedia articles and is an editor of two special issues on hearing aids and microphone arrays. He holds seven patents in the area of speech enhancement and microphone arrays. His main research efforts have been spent in the fields of speech enhancement, adaptive and optimum microphone arrays, audio signal processing, and acoustic communication.



**Zhiqiang He** (S'01–M'04) received the B.E. degree and the Ph.D. degree (Hons.) in signal and information processing from the Beijing University of Posts and Telecommunications, China, in 1999 and 2004, respectively. Since 2004, he has been with the School of Information and Communication Engineering, Beijing University of Posts and Telecommunications, where he is currently a Professor and the Director of the Center of Information Theory and Technology. He is also a Visiting Scholar with Xiamen University. His research interests include signal and information processing in wireless communications, networking architecture and protocol design, machine learning, and underwater acoustic communications.



**Alexander (Alec) J. Duncan** (M'92) was born in Melbourne, Australia, in 1958. He received the B.App.Sc. degree in applied physics from the Royal Melbourne Institute of Technology, Melbourne, VIC, Australia, in 1979, and the M.App.Sc. degree in applied physics (underwater acoustics) and the Ph.D. degree in underwater acoustics from Curtin University, Perth, WA, in 1988 and 2004, respectively.

From 1979 to 1980, he was a Development Engineer with Marconi Avionics, Basildon, U.K., and from 1980 to 1984, he was a Research Officer with the University of Bath, U.K. From 1980 to 1987, he was a Research Assistant with the Curtin University. From 1987 to 1991, he was with Internode Pty. Ltd., Melbourne, Australia, after which he moved back to Curtin University where he has involved in a number of different roles. He currently holds two positions at the university, where he is a Senior Research Fellow with the Center for Marine Science and Technology and a Senior Lecturer with the Department of Physics and Astronomy.

Dr. Duncan is a member of the Acoustical Society of America and the Australian Acoustical Society.